

Hydrodynamic propulsion of liposomes electrostatically attracted to a lipid membrane reveals size-dependent conformational changes

Seyed R. Tabaei^{†,‡,⊥}, Jurriaan J. J. Gillissen^{†,‡,⊥}, Stephan Block[¶], Fredrik Höök[¶], and Nam-Joon Cho^{*,†,‡,§}

[†]School of Materials Science and Engineering, Nanyang Technological University, 50 Nanyang Avenue 639798, Singapore

[‡]Centre for Biomimetic Sensor Science, Nanyang Technological University, 50 Nanyang Drive 637553, Singapore

[§]School of Chemical and Biomedical Engineering, Nanyang Technological University, 62 Nanyang Drive 637459, Singapore

[¶]Department of Applied Physics, Chalmers University of Technology, SE-412 96, Göteborg, Sweden

*E-mail: njcho@ntu.edu.sg

Abstract

The efficiency of lipid nanoparticle uptake across cellular membranes is strongly dependent on the very first interaction step. Detailed understanding of this step is in part hampered by the large heterogeneity in physicochemical properties of lipid nanoparticles, such as liposomes, making conventional ensemble-averaging methods too blunt tools to address details of this complex process. Here we contribute a new means to explore whether individual liposomes become deformed upon binding to fluid cell-membrane mimics. This was accomplished by using hydrodynamic forces to control the propulsion of nanoscale liposomes electrostatically attracted to a supported lipid bilayer (SLB). In this way, the size of individual liposomes could be determined by simultaneously measuring both their individual drift velocity and diffusivity, revealing that for a radius of ≈ 45 nm, a close agreement with dynamic light scattering data was observed, while larger liposomes (radius ≈ 75 nm) displayed a significant deformation unless composed of a gel-phase lipid. The relevance of being able to extract this type of information is discussed in the context of membrane fusion and cellular uptake.

Keywords: liposome deformation, single particle tracking, TIRF microscopy, supported lipid bilayer, hydrodynamic propulsion

50 **Introduction**

51 Liposomes (lipid vesicles) are self-closed spherically assembled lipid bilayers, that can be prepared
52 in a size range from around 20 nm up to several μm .^{1, 2} Morphologically they resemble cell
53 membranes and other naturally occurring particles such as transport secretory vesicles^{3, 4} and cell-
54 derived extracellular vesicles,⁵ as well as lipid enveloped viruses. Artificial liposomes are widely
55 used as model systems to study membrane-related processes⁶ and are more and more frequently
56 used as nano-containers in drug-delivery applications.⁷⁻⁹ Many studies reveal a critical influence of
57 liposome size on biological functions, such as enzymatic reaction kinetics,^{10, 11} protein binding¹²⁻¹⁴
58 and membrane-protein diffusivity in membranes.¹⁵ The size dependence of the above mentioned
59 phenomena has been primarily attributed to the stress in a curved membrane, which is related to the
60 area difference of the inner and the outer membrane leaflet, as well as to the mismatch between the
61 physical and spontaneous curvatures.^{16, 17} As the liposome size is reduced, the curvature
62 increasingly affects the conformations of the molecules that constitute the membrane, leading to
63 changes in both chemical and mechanical properties of the membrane.^{12, 18-20} It is therefore not
64 surprising that also drug encapsulation into liposomes²¹ as well as their uptake into cells have been
65 observed to depend on liposome size.²²⁻²⁶

66 Studying the aforementioned size-dependent phenomena is not trivial, though, and requires
67 methods that can independently determine both liposome size and biomolecular content with high
68 accuracy. When freely floating in a liquid, the size can be determined by measuring the diffusivity
69 D , which is equivalent, through Einstein's relation $\mu = k_{\text{B}}T/D$, to the friction coefficient μ , where
70 $k_{\text{B}}T$ is the Boltzmann energy, and then by applying the Stokes' drag law: $\mu = 6\pi\eta a$, one can translate
71 the diffusivity D into the radius a , via the celebrated Stokes - Einstein relation: $a = k_{\text{B}}T/6\pi\eta D$.
72 However, when liposomes are in a complex medium, e.g. porous^{27, 28} or non-Newtonian²⁹ or when
73 they are immobilized or move in a film or on a two-dimensional (2D) interface such as a cellular
74 membrane,³⁰⁻³⁴ then Stokes' drag law does not hold and measuring the diffusivity is insufficient to

75 determine the size. In such cases one needs to rely on indirect measures of liposome size, by e.g.
76 correlating lipid content with size,³⁵ while additional information is required to directly determine
77 the size or changes in size induced upon interactions occurring in complex matrices, e.g., upon
78 binding to a cellular membrane.

79 We here propose that by combining the above mentioned diffusion-based determination of
80 the friction coefficient with an independent measurement of the very same parameter, both the
81 absolute size and interaction-induced changes in size of membrane-adhering liposomes can be
82 determined. By applying a force F to a particle and measuring the induced drift velocity U , which is
83 the steady motion in a fixed direction, as opposed to random diffusive motion, the friction
84 coefficient, μ , can be determined using $\mu = F/U$. If the applied force is a known function of the
85 operating conditions, e.g., radius a , drift velocity U , etc., then the radius can be obtained by solving:

$$86 \quad F(a, U, \dots) = \frac{k_B T U}{D}. \quad (1)$$

87 Alternatively, when the radius is known, then other properties may be extracted from Eq. (1), such
88 as shape or electric charge. For instance Yoshina-Ishii *et al.*³⁶ determined the electrophoretic
89 mobility by measuring the electro-osmotically induced drift velocity and diffusivity of individual
90 negatively charged liposomes, that were tethered using DNA strands to a negatively charged lipid
91 bilayer. Jönsson *et al.*³⁷ determined the shape of proteins, by measuring the shear-induced drift and
92 diffusivity of fluorescently labeled membrane-adhering proteins, while Block *et al.* recently
93 demonstrated that both liposome size and fluorescence emission intensity can be independently
94 determined by using Eq. (1) in combination with measurements of both U and D ³⁸ and that the
95 number of linkers between a liposome and a membrane can be extracted from D alone.³⁹

96 The above mentioned studies demonstrate the potential of combined diffusivity and drift
97 velocity measurements to extract properties of particles that are confined to a mobile interface, but
98 did not specifically address that liposomes may deform in response to interfacial interactions, as
99 previously observed at solid interfaces.⁴⁰⁻⁴⁶ Inspired by the design of lipid nanoparticles that has

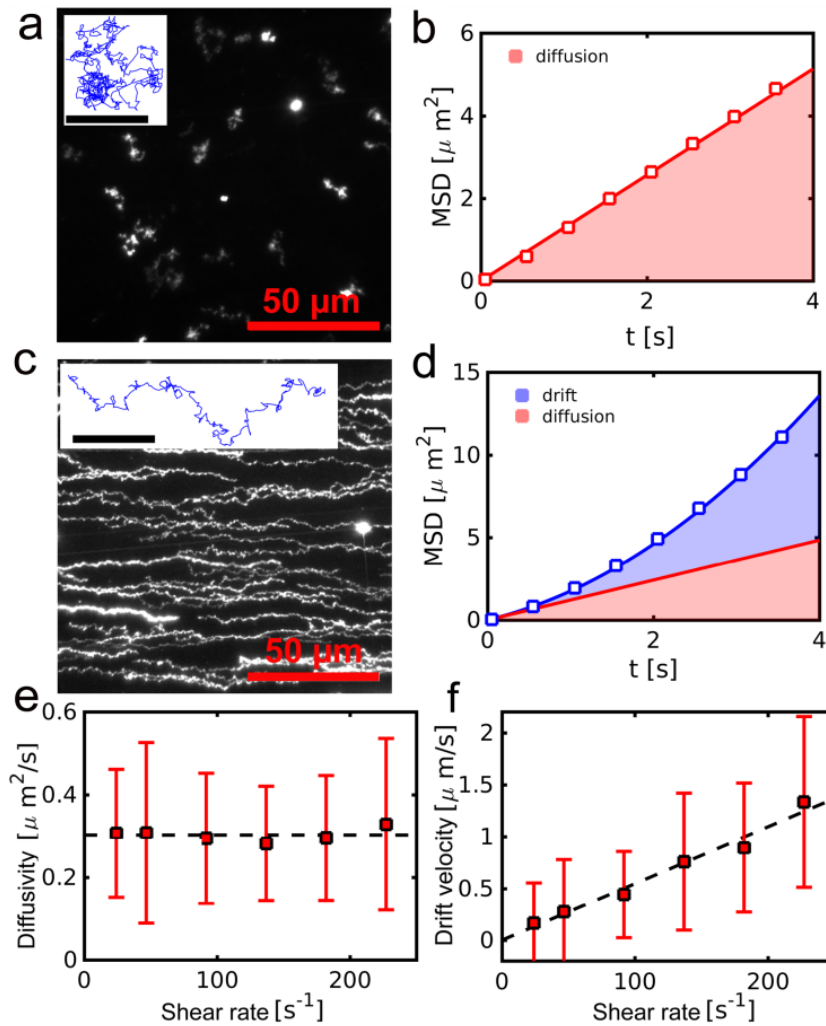
100 been proven efficient in various drug delivery applications, we here apply this approach to
101 determine both the size and conformational changes of individual membrane-adhering liposomes
102 induced by direct membrane-membrane interactions controlled by electrostatic attraction between
103 oppositely charged lipid bilayers in close contact.^{47, 48} The observed dependence of liposome
104 deformation on size and membrane rigidity is discussed in the context of understanding how to
105 optimize lipid nanoparticle formulations.

106 **Results and Discussion**

107 A positively charged supported lipid bilayer (SLB) [PC:EPC (90:10)] was formed using the vesicle
108 fusion method in a fluidic chamber, with width $W = 3.8$ mm, height $H = 0.4$ mm and length of $L =$
109 17 mm. Negatively charged liposomes (radius $a \approx 45$ nm) [PC:PS (95:5)] were fabricated by the
110 extrusion method. After injection into the flow chamber, the liposomes spontaneously adhered
111 electrostatically onto the SLB, where they were observed to diffuse in 2D (see Supporting Video
112 S1). Prior to injection, the liposome radius distribution was measured using dynamic light scattering
113 (DLS). In Figure 1a, we visualize the diffusive motions of the liposomes by superimposing 350
114 images taken by fluorescence microscopy, which correspond to a time lapse of 17.5 s. We used
115 particle tracking to reconstruct the liposome trajectories. An example trajectory is displayed in the
116 inset of Figure 1a. To quantify the diffusion the mean squared displacement (MSD) between all
117 point-pairs on the trajectory as a function of the time separation between the paired points was
118 calculated. The (MSD) in Figure 1b was fitted by Eq. (5) (see Experimental Section), which gives a
119 diffusivity of: $D = 0.25 \mu\text{m}^2 \text{s}^{-1}$. Since the trajectory in the inset of Figure 1a, is relatively long, the
120 uncertainty in the fitted D is small (<1%), i.e. the MSD follows Eq. (5) within 1%. For relatively
121 short trajectories on the other hand, the uncertainty may be larger, and we exclude short trajectories
122 with an uncertainty in the fitted D above 3%.

123

124



125

126 **Figure 1.** Liposome motion visualized by the superposition of 350 fluorescence images without
 127 applied flow (a) and with applied flow, corresponding to a shear rate of $\gamma = 227 \text{ s}^{-1}$ (flow rate: $\Phi =$
 128 $23 \text{ }\mu\text{L/s}$) (c). For each case a reconstructed trajectory is shown as an inset (the scale bar in the insets
 129 corresponds to $5 \text{ }\mu\text{m}$) and the corresponding mean squared displacements (MSDs) are shown as a
 130 function of the elapsed time t in (b) and (d). Without applied flow, the liposome motion is purely
 131 diffusive and the MSD is linear (shaded red). With applied flow, the liposome motion includes a
 132 substantial drift, reflected by the quadratic part of the MSD (shaded blue). (e) Mean and standard
 133 deviation of the diffusivity D as functions of the shear rate γ . (f) Mean and standard deviation of
 134 the drift velocity U as functions of γ . Please note that the data in (e) and (f) are ensemble averaged
 135 over all detected trajectories, while the data in (b) and (d) correspond to a single trajectory only.
 136

137 Next aqueous buffer solution was injected into the chamber (see Supporting Video S2).

138 Figure 1c, shows the resulting motion of the membrane-adhering liposomes (volumetric flow
 139 velocity: $\Phi = 23 \text{ }\mu\text{L/s}$). The liposome motion was again visualized by overlaying 350 fluorescence
 140 images, covering a total time lapse of 17.5 s. The figure shows that in addition to diffusive motion,
 141 the particles show a horizontally directed motion (drift). The inset of Figure 1c shows a
 142 reconstructed liposome trajectory, and the corresponding mean squared displacement is shown in

143 Figure 1d. In comparison to the MSD without shear (Figure 1b), the MSD in Figure 1d has an
 144 additional, quadratic component, which corresponds to the drift velocity. By fitting Eqs. (4) and (5)
 145 to the data in Figure 1d, the drift velocity and diffusivity were determined to be $U = 0.8 \mu\text{m}\cdot\text{s}^{-1}$ and
 146 $D = 0.25 \mu\text{m}^2\cdot\text{s}^{-1}$, respectively. For the case presented in Figure 1d the uncertainties in the fitted U
 147 and D are small ($<1\%$), i.e. the mean displacement and the mean squared displacement are within
 148 1% of Eqs. (4) and (5), respectively. Again it is noted that only sufficiently long trajectories are
 149 considered in the analysis such that uncertainties in U and D are below 3%. Following this
 150 approach, we determined U and D for about 50 liposome trajectories, reconstructed from the
 151 fluorescence image sequence. To study the effect of the flow rate on the diffusivity and on the drift
 152 velocity, we repeated the experiment with different flow rates (Φ between 0 and $23 \mu\text{L}\cdot\text{s}^{-1}$).

153 The fluid velocity experienced by the liposomes equals γa where a is the liposome radius
 154 and γ is the fluid shear rate at the membrane surface, which is the increase of the fluid velocity per
 155 unit length when moving away from the surface. The shear rate is related to the flow rate by: $\gamma = 6\Phi$
 156 $/WH^2$ and has been varied between 0 and 227s^{-1} in the present work. In Figure 1e we observe that
 157 changing the shear rate γ in this range has no marked effect on the liposome diffusivity, which
 158 remains at a constant value of: $D = 0.30 \pm 0.1 \mu\text{m}^2\cdot\text{s}^{-1}$. The drift velocity U on the other hand
 159 depends linearly on the shear rate γ (Figure 1f). These observations support the view that the
 160 friction coefficient between the liposome and the shear flow and the friction coefficient between the
 161 liposome and the underlying membrane are both insensitive to the applied shear rate, i.e. they are
 162 insensitive to the speed of the liposome.

163 Now we will use Eq. (1) to determine the size (radius a) of individual membrane-adhering
 164 liposomes. To this end we use the following, generally valid expression, for the shear-induced
 165 friction force.

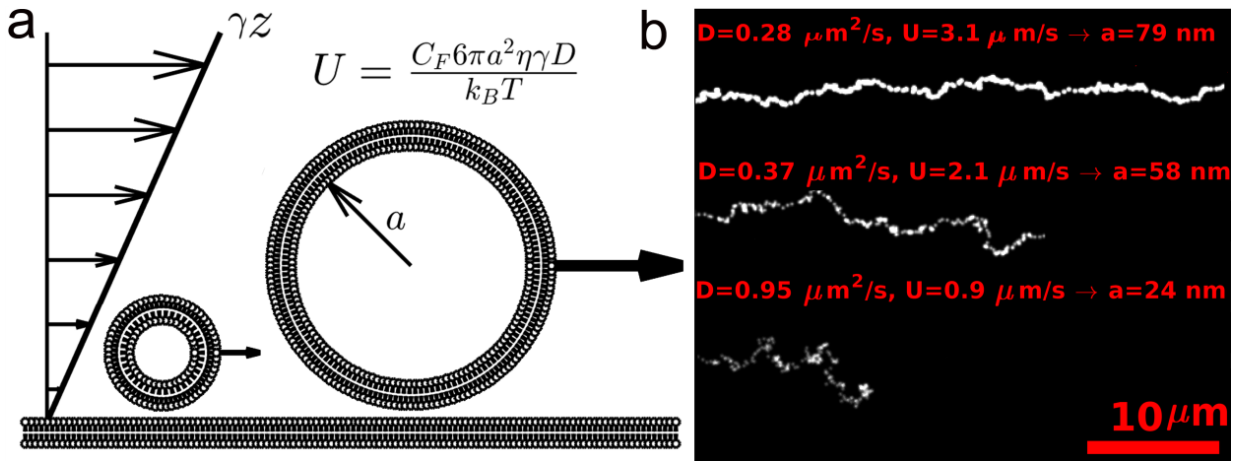
$$166 \quad F = C_F 6\pi\eta a^2 \gamma. \quad (2)$$

167 Here η is the solvent dynamic viscosity and C_F is the *solvent friction factor*. For solid spheres: $C_F \approx$

168 1.7,⁴⁹ while for other shapes or fluid-like particles, C_F may take on other values. For instance, C_F
169 decreases when the liposome shape deforms from spherical to ellipsoidal, under constant area $A =$
170 $4\pi a^2$, *i.e.*, with constant effective radius a .³⁷ Therefore, C_F is a measure for the shape of an object, a
171 property that we will exploit later on. Inserting Eq. (2) into Eq. (1) results in:

$$172 \quad a = \sqrt{\frac{k_B T U}{C_F 6 \pi \eta \gamma D}}. \quad (3)$$

173 For the derivation of Eq. (3) it has been used that the liposomes move much faster than the SLB,
174 which itself is also being pushed forward by the shear flow, while at the same time, the liposomes
175 move much slower than the fluid, *i.e.* the friction between the liposomes and the SLB is much larger
176 than the friction between the liposomes and the solvent. A full derivation and a discussion of these
177 assumptions are presented in the Supporting Information, showing that the SLB moves 100 times
178 slower than the liposomes, which in turn move 10 times slower than the local fluid. Eq. (2)
179 suggests that larger particles move faster, since they experience a larger hydrodynamic force from
180 the shear flow (Figure 2a). To illustrate the size dependent dynamics, we have plotted in Figure 2b,
181 the trajectories for three liposomes emitting markedly different fluorescence intensities. For each
182 liposome, the measured diffusivity D and velocity U are given, and the radius a , as predicted by Eq.
183 (3), is seen to correlate well with the observed fluorescence intensity, which is an alternative
184 (control) size measurement, as discussed below. Figure 2b furthermore indicates that with
185 increasing radius, the drift velocity increases and the diffusivity decreases, resulting in trajectories
186 that are less random and more directed.



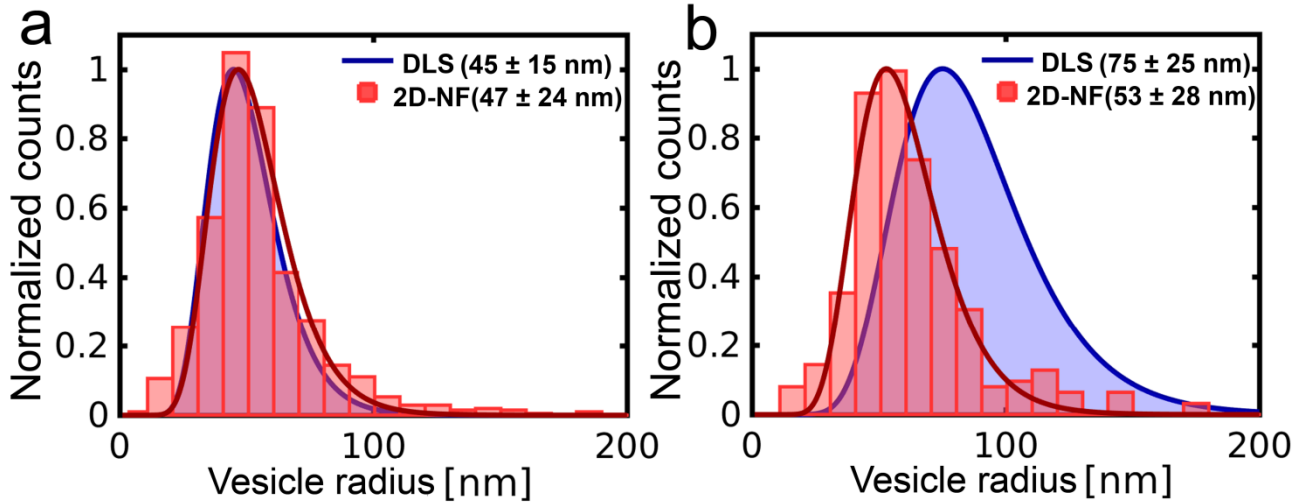
187
188
189
190
191
192
193

Figure 2. Illustration of the size (radius a) dependent drift velocity. **(a)** Cartoon of the shear-induced propulsion of differently sized liposomes. **(b)** Trajectories, measured with fluorescence microscopy, for three differently-sized liposomes. The trajectories are superpositions of diffusion and drift velocity. As the radius of the liposome increases, the drift component increases and the trajectories become less random and more directed.

194 Using the measured drift velocity and diffusivity and assuming that $C_F \approx 1.7$ (solid sphere
195 behavior), Eq. (3) predicts the radius a of the individual liposomes. We refer to this method as “two
196 dimensional flow nanometry” (2D-FN). The corresponding radius distribution is shown in Figure
197 3a, where, for the sake of having sufficient statistics, data for all flow rates have been combined.
198 We will discuss the effect of the flow rate on the accuracy of the method below. In Figure 3a we
199 also plot the radius distribution obtained from dynamic light scattering (DLS). There is nearly
200 perfect agreement between both distributions, which validates that the hydrodynamic interaction
201 between the liposomes and the shear flow resembles that of solid spheres: $C_F \approx 1.7$.

202 This remarkable observation supports the notions that the small (fluid phase) liposomes
203 (radius ≈ 45 nm) (i) experience a negligible amount of flow in the lipid membrane, i.e. they impose
204 a no-slip boundary condition to the surrounding fluid, similar as for solid particles and (ii) they do
205 not deform significantly upon adsorption on the membrane surface and remain spherical. The
206 condition of negligible membrane flow is in line with the (successful) use of Stokes’ relation (valid
207 for solid spheres) when determining liposome size by measuring the diffusivity.⁵⁰ The apparent
208 spherical shape of the adsorbed liposomes implies that the bending energy dominates the substrate-
209 induced adhesion energy.⁵¹ In the literature liposome deformation has been observed on solid

210 surfaces, suggesting a large substrate-induced adhesion energy (compared to the bending energy).⁴¹,
 211 ⁵² Our result of a negligible deformation of small liposomes (radius ≈ 45 nm) on a fluid membrane
 212 interface (Figure 3a) suggests that the inter-membrane adhesion energy for these liposomes is small
 213 compared to the bending energy.

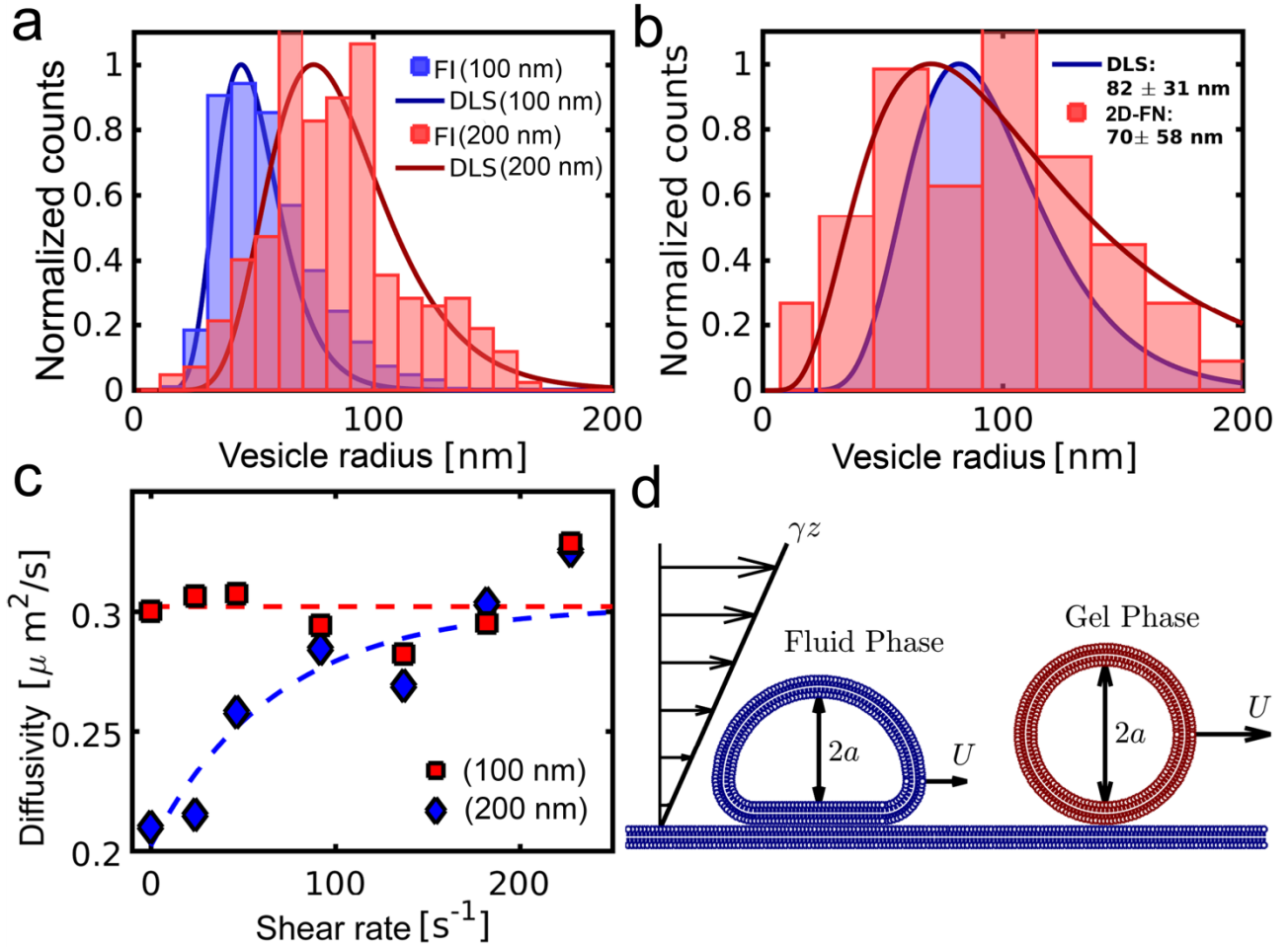


214

215 **Figure 3.** Radius distribution of membrane-adhering liposomes obtained from 2D flow nanometry
 216 [2D-FN, Eq. (3)] (red; bars) and obtained from dynamic light scattering (DLS, blue) (a) for small
 217 liposomes (extruded through 100 nm pores) and (b) for large liposomes (extruded through 200 nm
 218 pores). The legends indicate the mode and the standard deviation of the respective distributions.
 219

220 However with increasing liposome radius a the adhesion energy is expected to increase in
 221 proportion to the liposome contact area $\sim a^2$, while the bending energy is independent of a .^{51, 53}
 222 Therefore larger membrane-adhering liposomes are expected to be more prone to shape
 223 deformation.^{54, 55} Such shape deformation would affect the hydrodynamic coupling between the
 224 shear flow and the liposome,³⁷ and to explore this effect, we studied a second batch of larger
 225 liposomes (radius $a \approx 75$ nm). Henceforth we refer to these liposomes ($a \approx 75$ nm), as the “large
 226 liposomes”, while the ones with $a \approx 45$ nm are referred to as the “small liposomes”. Similar to the
 227 case of the small liposomes, we measured the drift velocity and the diffusivity of the large
 228 liposomes at various shear rates and computed the radii of the individual liposomes using Eq. (3).
 229 The resulting radius distribution together with the corresponding DLS data is shown in Figure 3b. It
 230 is seen that the radius of the large liposomes on the membrane surface (measured by 2D-FN) is
 231 smaller than the corresponding values in bulk (measured by DLS). This result indicates that the

232 large liposomes are flattened, resulting in a reduced shear-induced propulsion force, as compared to
 233 spherical liposomes (with the same surface area). As an effect the flattened liposomes move slower
 234 than the spherical liposomes and appear to be smaller than their actual size in the “eyes” of 2D-FN.



235
 236 **Figure 4.** (a) The radius distribution obtained from the square root of the fluorescence intensity
 237 (FI; bars) and obtained from dynamic light scattering (DLS; lines) for small (extruded through 100
 238 nm pores; blue) and large (extruded through 200 nm pores; red) liposomes. (b) Radius distribution
 239 for large membrane-adhering, gel phase liposomes, obtained from particle tracking on the
 240 membrane interface [Eq. (3)] (red bars) and obtained from DLS (blue). The legends indicate the
 241 mode and the standard deviation of the respective distributions. (c) Liposome diffusivity as a
 242 function of the shear rate for small liposomes (extruded through 100 nm pores; red squares) and
 243 large liposomes (extruded through 200 nm pores; blue diamonds). (d) Schematic representation
 244 illustrating that the large fluid-phase liposomes deform and therefore move slower than their
 245 undeformed, gel-phase counterparts.
 246

247 We verified that the DLS radius distribution, which was measured for suspended liposomes,
 248 is representative for the liposome radius distribution on the membrane surface. To this end we
 249 compared the DLS radius distribution to that of the square root of the fluorescence intensity $I^{1/2}$,

250 emitted by individual membrane-adhering liposomes. This quantity is converted to radius, where
251 the conversion factor is found, by matching the peak of the $I^{1/2}$ distribution to that of the DLS.^{35, 56}
252 Figure 4a shows the resulting distributions, where we have used *the same conversion factor*, for
253 both small and large liposomes. The observation that both resulting distributions closely follow the
254 DLS data strongly supports that DLS is representative for the liposomes on the membrane surface,
255 and therefore suitable to validate the radius distributions obtained using 2D-FN (Figures 3a and 3b).

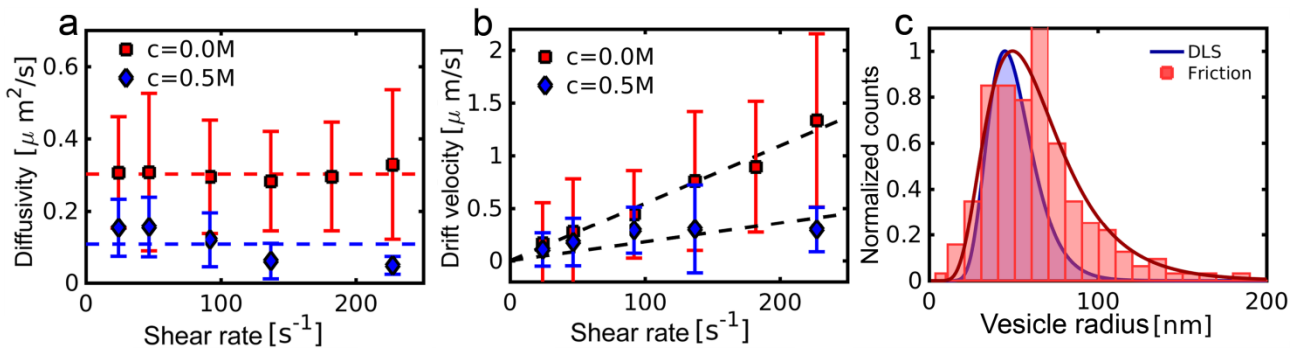
256 We therefore hypothesize that the deviation with regards to radius determination using 2D-
257 FN flow nanometry and DLS observed for large liposomes (Figure 3b) is due to liposome
258 deformation. To confirm this hypothesis, we conducted a control 2D-FN experiment, using large
259 liposomes (radius ≈ 82 nm) composed of DPPC (1,2-dipalmitoyl-*sn*-glycero-3-phosphocholine),
260 with a gel to liquid transition temperature of $\approx 40^\circ\text{C}$,⁵⁷ and 5 mol% negatively charged DOPS
261 lipids. The bending energy at room temperature of DPPC ($\approx 250 k_B T$)⁵⁸ is an order of magnitude
262 larger than that of DOPC ($\approx 25 k_B T$)⁵⁹, and the gel phase DPPC liposomes are therefore expected to
263 be less prone to deformation. The resulting 2D-FN radius distribution is compared to the
264 corresponding radius distribution obtained from DLS in Figure 4b, which shows a good agreement
265 between both distributions. The peaks of the distributions are within 10 nm of each other. The
266 improved agreement between 2D-FN and DLS when going from fluid-phase (Figure 3b) to gel-
267 phase (Figure 4b) liposomes strongly supports the hypothesis that the deviation between the radius
268 determination made from 2D-FN and DLS (Figure 3b) is due to deformed shapes of the large fluid-
269 phase liposomes.

270 Deformation of the large liposomes is further supported by the observation that their
271 diffusivity increase with the applied shear-rate, as shown in Figure 4c. This observation implies that
272 with increasing liposome velocity, there is a reduced friction coefficient between the liposomes and
273 the membrane surface. This effect may be caused by an increase of the inter-membrane separation,
274 due to a shear-induced lift force. The shear-induced lift force requires a non-spherical liposome

275 shape,⁶⁰ *i.e.* it vanishes (relative to the drag force) for spheres at small Reynolds numbers $Re = a^2\gamma/\nu$
276 $\sim 10^{-6}$,⁶¹ where ν is the solvent kinematic viscosity. In the supporting information, we analyze the
277 relation between the inter-membrane separation and the diffusivity of the membrane-adhering
278 liposomes. The analysis shows, that a very small increase in the separation (~ 0.4 nm) causes a very
279 large increase in the diffusivity (~ 50 %). This sensitivity towards the inter-membrane spacing
280 supports the notion that a shear-induced lift force acts on the large liposomes, resulting in the
281 observed increase in the diffusivity with increasing shear rate (Figure 4c). This in turn supports our
282 hypothesis that the large liposomes are deformed since non-sphericity is required to generate a
283 shear-induced lift force. For the small liposomes on the other hand, the observed diffusivity is
284 independent of the shear rate (Figure 1e), which is consistent with a spherical liposome shape.
285 Figure 4d presents a cartoon to illustrate that the deformation of large, fluid-phase vesicles results in
286 a smaller drift velocity as that of their gel-phase counterparts.

287 To further study the relation between the inter-membrane friction and the adhesion force we
288 changed the latter by adding 500 mM glucose to the solvent, which is non-permeable to the
289 membrane. Due to their relatively large size (1.5 nm), the glucose molecules are expected to be (at
290 least partly) depleted from the (1 nm) inter-membrane hydration layer and thereby enhance the
291 inter-membrane friction due to a depletion force.^{36, 62} In addition to the depletion force, the glucose
292 molecules also exert an osmotic pressure, which may deform the liposomes. This would also result
293 in an enhanced inter-membrane friction, through an extended contact area. We used the 2D-FN
294 method to shed light on these processes by probing not only the inter-membrane friction, but also
295 liposome deformation, via the change in the hydrodynamic radius. For this experiment we used the
296 small liposomes, which are non-deformed in the absence of glucose (see Figure 3a). Figure 5a
297 shows that in the presence of glucose, the small liposomes have a 50 % smaller diffusivity: $D =$
298 $0.16 \pm 0.18 \mu\text{m}^2\cdot\text{s}^{-1}$ as compared to the case without glucose, where: $D = 0.30 \pm 0.18 \mu\text{m}^2\cdot\text{s}^{-1}$. This
299 decrease in diffusivity corresponds to a doubling of the inter-membrane friction force, while

300 changes in bulk viscosity (10 %) are of minor importance.⁶³ The larger inter-membrane friction is
 301 furthermore reflected by a smaller drift velocity, shown in Figure 5b. Despite the substantially
 302 larger inter-membrane friction, the radius distribution obtained from 2D-FN [Eq. (3)] is still in good
 303 agreement with the DLS data (Figure 5c), which means that the liposomes remain spherical upon
 304 adding 500 mM glucose, and that the observed reduced diffusivity is most likely the effect of an
 305 enhanced inter-membrane friction due to a depletion force. While large liposomes (radius ~ 100
 306 nm) are known to shrink upon exposure to a hyperosmotic solution,^{64, 65} we do not observe osmotic
 307 volume change for small liposomes (radius ≈ 45 nm), nor has this been reported in the literature.⁶⁶

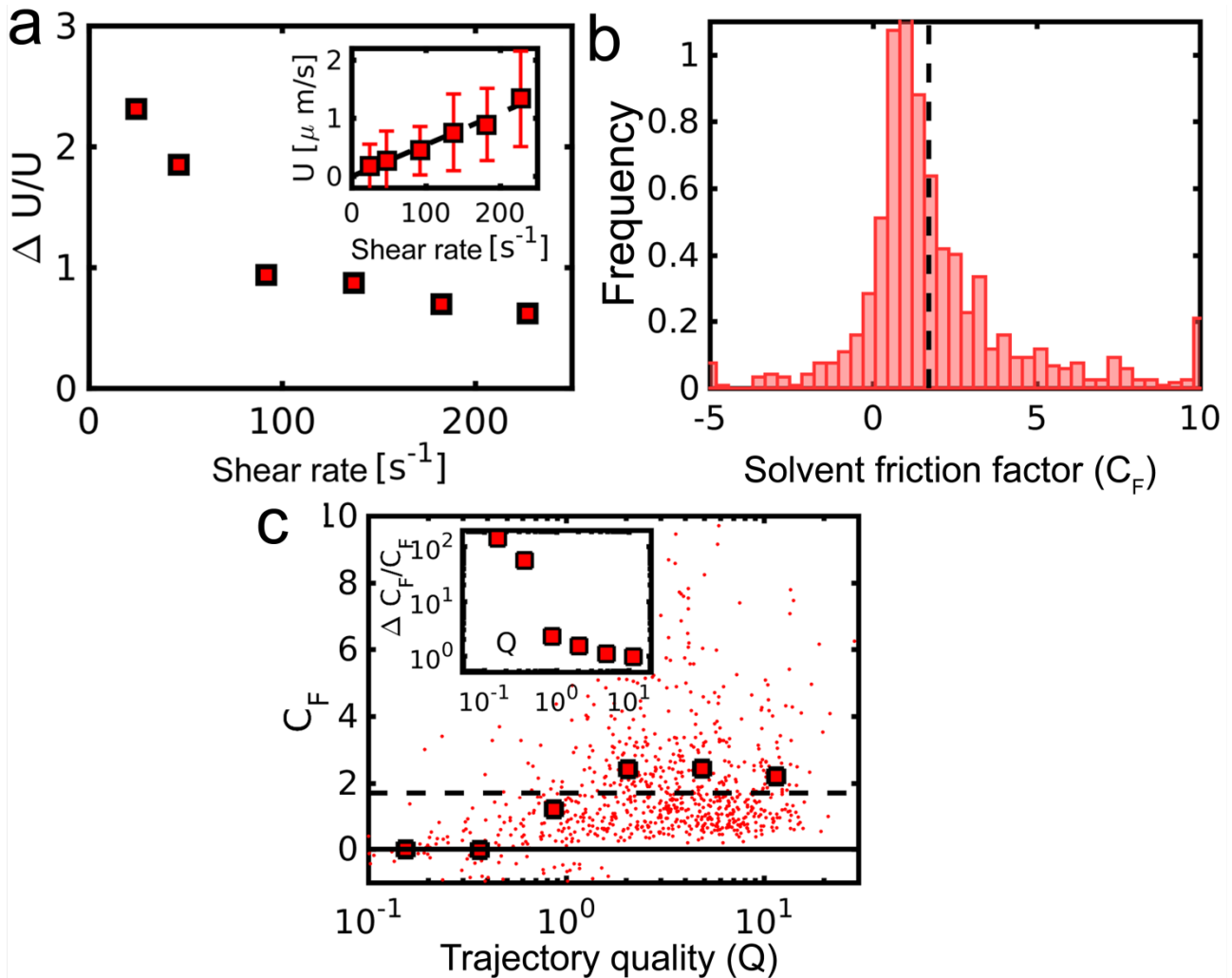


308
 309 **Figure 5.** Effect of glucose on the hydrodynamic propulsion of the small liposomes. **(a)** Mean
 310 (markers) and standard deviation (error bars) of the liposome diffusivity D as functions of the shear
 311 rate γ with 500 mM glucose in solution (blue diamond) and without glucose in solution (red square).
 312 **(b)** Mean and standard deviation of the liposome drift velocity U as functions of the shear rate γ
 313 with 500 mM glucose in solution (blue diamond) and without glucose in solution (red square). **(c)**
 314 Radius distribution of membrane-adhering liposomes in 500 mM glucose solution, obtained from
 315 particle tracking on the supported lipid membrane [Eq. (3)] (red; bars) and obtained from DLS
 316 (blue).
 317

318 Finally we discuss the accuracy of the method. Figure 6a shows (for the small liposomes)
 319 that the relative spread in the measured drift velocity $\Delta U/U$ depends inversely on the applied shear
 320 rate γ for small $\gamma < 100 \text{ s}^{-1}$, while for large $\gamma > 100 \text{ s}^{-1}$, $\Delta U/U$ approaches a plateau value that is
 321 independent of γ . This observation indicates that $\Delta U/U$ is composed of a stochastic component,
 322 which decreases with increasing drift velocity and a material component that is independent of the
 323 drift velocity. The material component reflects variations in the liposome radius, *i.e.*, large
 324 liposomes move faster than small liposomes, as well as variations in the liposome shape and

325 composition, such as charge or multilamellarity.

326



327 **Figure 6.** Accuracy of the 2D flow nanometry (2D-FN) method, to determine the radius of the small
 328 liposomes. **(a)** Relative standard deviation of the liposome drift velocity U as a function of the
 329 applied shear rate γ . The inset shows the liposome drift velocity as a function of the applied shear
 330 rate γ . **(b)** Distribution of the solvent friction factor: $C_F = k_B T U / (6\pi a^2 \eta \gamma D)$. The vertical, dashed
 331 line corresponds to the theoretical value for solid spheres: $C_F = 1.7$. **(c)** Scatter plot of C_F versus the
 332 trajectory quality: $Q = U(t/D)^{1/2}$. Each dot corresponds to one trajectory. The large markers
 333 represent the mean of C_F as a function of Q . The inset shows the relative standard deviation of C_F
 334 versus Q .
 335
 336

337 To study the accuracy of the method, we compute the solvent friction factor C_F for each individual
 338 liposome, by inserting the measured values for radius (obtained from fluorescence intensity),
 339 diffusivity and drift velocity into Eq. (3). While, perfect accuracy correspond to all liposomes
 340 giving exactly: $C_F = 1.7$, we find a distribution with: $C_F = 2.1 \pm 3.9$. Figure 6b shows the

341 corresponding histogram. Despite the large spread, the mean value is surprisingly close to the
342 theoretical value for solid spheres: $C_F = 1.7$. The observed spread is the accumulation of the spread
343 of the depending variables, *i.e.* liposome radius, diffusivity and drift velocity U . In the Supporting
344 Information, we argue that the measurement uncertainty in the drift velocity U , due to the stochastic
345 nature of the diffusion process, is given by: $\Delta U/U \sim (D/U^2t)^{1/2}$, which means that the accuracy of
346 the method improves for large values of the so-called trajectory quality Q :

$$347 \quad Q = \sqrt{\frac{U^2t}{D}}. \quad (4)$$

348 Here t refers to the total time of the trajectory. We verify this in Figure 6c, by showing C_F as a
349 function of Q , where each marker corresponds to one trajectory. This figure compiles data for all
350 the different shear rates. The large markers correspond to the mean C_F , as a function of Q . This
351 figure shows that for small trajectory quality: $Q \lesssim 1$, the solvent friction factor C_F is distributed
352 around zero, in contrast to the theoretical value of 1.7, while for large trajectory quality: $Q \gtrsim 1$, the
353 mean of C_F approaches the theoretical value of 1.7. The inset of Figure 5c shows the relative
354 standard deviation $\Delta C_F/C_F$, which is a measure for the uncertainty of the present size determination
355 method. The data show that with increasing Q , the uncertainty decreases and reaches a plateau
356 value, which supports the notion that for $Q \gtrsim 1$, the uncertainty of the method is no longer
357 governed by the stochastic nature of the diffusion process, but rather by deviations in liposome size,
358 shape and chemical composition. In summary the successful application of the 2D-FN method
359 requires a sufficiently large flow rate, $Q \gtrsim 1$, to allow an accurate determination of the drift
360 velocity. This requirement must be met under the restrictions of having sufficient ($\gtrsim 100$) samples
361 per trajectory, to allow tracking of the particle and to ensure an accurate determination of the
362 diffusivity. Additionally, the liposome surface coverage must be sufficiently small, such that
363 individual liposomes can be tracked over the full width of microscopy image. With regard to
364 accuracy it is further noted that the method is limited to sufficiently large particles, since their
365 velocity must be much larger than the shear-induced velocity of the membrane, such that the latter

366 can be ignored in the analysis. We have shown in the Supporting Information, that this condition is
367 met in the current system. For smaller particles however, like, say proteins, [Ref. Jönsson, P.;
368 Jönsson, B. *Langmuir* 2015, 31, 12708-12718] this condition will be violated. This problem could
369 be remedied by using anchored lipid bilayers [references] or lipid monolayers on hydrophobic
370 supports. [references]

371 **Conclusions**

372 In summary, we have measured the shear-induced drift velocity U and diffusivity D of membrane-
373 adhering liposomes. The radii of the liposomes were determined by combining U and D with the
374 Einstein relation for diffusion, under the assumption that the hydrodynamic propulsion force
375 resembles that on solid spheres. For small liposomes (effective radius of ≈ 45 nm) the resulting
376 radius distribution agrees well with DLS measurements, confirming liposome sphericity, while
377 deviations for large fluid phase liposomes (effective radius of ≈ 75 nm) suggest liposome
378 deformation at the membrane interface. The method thus offers a means to measure liposome
379 deformation at a mobile interface, which is particularly relevant in the context of understanding the
380 interaction between liposomes and cellular membranes. In this context, computer simulations of the
381 translocation of nanoparticles across lipid bilayers predicted a better penetrability for elongated
382 particle shapes.⁶⁷ In addition, a higher membrane association as well as a faster cellular uptake have
383 been reported for elongated particles in comparison to their spherical counterparts.^{68, 69} Thus if we
384 solely consider the shape effects, deformation of large liposomes at the membrane interface could
385 promote their cellular entry. On the other hand, lipid exchange and membrane fusion may occur
386 during liposome-cell interactions.^{70, 71} These processes have been shown to be promoted by
387 increased membrane curvature⁷² due to a lowering of the free energy barrier of fusion intermediate
388 structures.^{73, 74} Thus, liposome deformation at the membrane interface may hinder fusion and inter-
389 membrane lipid exchange, which may rather hamper cellular uptake. We thus envision that the
390 approach presented in this work will contribute crucial information, that will help unraveling the

391 details of these complex processes, that determine the fate of cellular uptake of nanoparticles in
392 general and lipid nanoparticles in particular. Specifically, since nanometer scale deformations of
393 liposomes and variations in their interaction strength with cellular membranes can be determined
394 for individual liposomes, future studies on cellular uptake of liposomes of different size and rigidity
395 and their interfacial interactions with cell membrane should provide entirely new information
396 regarding the importance of shape deformations at the membrane interface for these very often
397 highly heterogeneous systems. This information could thereby serve as design principle for
398 developing more effective liposomal nanocarriers for drug delivery applications. It is also
399 worthwhile to note, that although hitherto unique as tool to explore deformation of individual
400 vesicles, AFM will inevitably push the laterally mobile vesicles, which thus risk becoming
401 “invisible”. These limitations were here overcome by applying a shear flow, which from optical
402 imaging and single particle tracking made it possible to quantify binding-induced deformation of
403 individual vesicles with sub 10 nm resolution. We thus expect the 2D flow nanometry concept to
404 contribute novel insights regarding both nanoparticle deformation and to map the adhesion and
405 binding energies of nanoparticles on mobile interfaces.

406 **Experimental Section**

407 **Liposome preparation.** Small unilamellar liposomes are fabricated from 1 % fluorescently labeled
408 1,2-dioleoylsn-glycero-3-phosphoethanolamine-N-(lissamine rhodamine B sulfonyl) (rhodamine-
409 PE) lipids, 5 % negatively charged 1-palmitoyl-2-oleoyl-sn-glycero-3-phospho-L-serine (sodium
410 salt) (DOPS) lipids and either 94 % zwitterionic 1-palmitoyl-2-oleoyl-sn-glycero-3-phosphocholine
411 (DOPC) lipids or 94 % 1,2-dipalmitoyl-sn-glycero-3-phosphocholine (DPPC) lipids by extrusion
412 above the gel to liquid-crystal transition temperature through membranes with either 100 nm or 200
413 nm pores. Liposomes are formed in aqueous buffer solution (10 mM Tris [pH 7.5] with 150 mM
414 NaCl).

415 **SLB formation and liposome adsorption.** Supported lipid bilayers (SLBs) are produced from 10

416 % positively charged 1,2-distearoyl-sn-glycero-3-ethylphosphocholine (chloride salt) (DOEPC)
417 lipids and 90 % zwitterionic DOPC lipids by the vesicle fusion method on the inner glass wall of a
418 micro-fluidic channel, with a length, width W and height H of 17, 3.8 and 0.4 mm, respectively.
419 After bilayer formation, liposomes are injected into the channel, which electrostatically adhere to
420 the positively charged supported lipid bilayer, resulting in a relatively low coverage of
421 approximately one liposome per $400 \mu\text{m}^2$, allowing the tracking of individual liposomes. After
422 liposome deposition, the channel is rinsed with buffer solution to eliminate liposomes in the bulk
423 obscuring the subsequent imaging. A hydrodynamic flow is applied to induce drift velocity of the
424 membrane-adhering liposomes. The flow rate is varied from $\Phi = 0.84 \text{ mm}^3 \cdot \text{s}^{-1}$ up to $23 \text{ mm}^3 \cdot \text{s}^{-1}$,
425 which corresponds to a shear rate from $\gamma = 6\Phi/H^2W = 8.3 \text{ s}^{-1}$ up to 227 s^{-1} .

426 **Fluorescence microscopy.** The motion of liposomes on SLBs were observed using a fluorescence
427 microscope with an inverted Eclipse TE 2000 microscope (Nikon) equipped with a high-pressure
428 mercury lamp, a $60\times$ oil objective (NA 1.49) and an Andor iXon+ EMCCD camera (Andor
429 Technology, Belfast, Northern Ireland). The acquired images consisted of 512×512 pixels with a
430 pixel size of $0.267 \times 0.267 \mu\text{m}$, which is equivalent to an image size of $137 \times 137 \mu\text{m}$. During flow,
431 a total of 350 fluorescence images are taken over a period of 17.5 s with a frame rate of 20 s^{-1} .

432 **Liposome tracking.** In the fluorescence images, liposomes are identified as clusters of more than
433 three and less than 100 pixels, whose fluorescence intensities exceeds two times the intensity noise
434 level. Assuming a constant surface number density of the fluorescence molecules within the
435 liposome membranes, the radius of an individual liposome can be estimated from the square root of
436 the fluorescence $I^{1/2}$ emitted by the liposome. The proportionality constant between liposome radius
437 and $I^{1/2}$ is determined by matching the peak of the resulting radius distribution to that obtained from
438 dynamic light scattering (DLS) experiments (Malvern Instruments, UK). Liposome positions in
439 subsequent frames are matched to construct liposome trajectories. A trajectory is terminated when
440 the liposome displacement exceeds five pixels or when the liposome comes within five pixels of

441 another liposome. In order to determine liposome diffusivity and drift velocity from the trajectory,
442 we compute for each trajectory the horizontal (flow direction) mean displacement $\overline{\Delta x}$ and the
443 horizontal plus vertical mean squared displacement $\overline{\Delta r^2} = \overline{\Delta x^2} + \overline{\Delta y^2}$ as functions of the elapsed
444 time t . For particles moving on a plane, with (horizontal) drift U and diffusivity D , these quantities
445 evolve as:

$$446 \quad \overline{\Delta x} = Ut, \tag{4}$$

447 and:

$$448 \quad \overline{\Delta x^2} + \overline{\Delta y^2} = 4Dt + U^2t^2. \tag{5}$$

449 Measured mean displacement and mean squared displacement are fitted to Eqs. (4) and (5), which
450 provides the liposome velocity U and diffusivity D . In the analysis we only consider trajectories that
451 are within 3% of the theoretical predictions [Eqs. (4) and (5)]. We also ignore liposomes that are
452 stagnant, i.e. when the diffusivity or the velocity is less than 100th of the respective mean value.

453 **Associated Content**

454 **Supporting Information**

455 Supporting Information contains additional details about relation between radius, drift and
456 diffusivity as well as 2D-FN accuracy.

457

458 This material is available free of charge via the Internet at <http://pubs.acs.org>

459

460 **Author Information**

461 **Corresponding Author**

462 *E-mail: njcho@ntu.edu.sg

463 **Author Contributions**

464 [†]These authors contributed equally to this work.

465 **Notes**

466 The authors declare no competing financial interest

467

469 **Acknowledgements**

470 We would like to gratefully acknowledge support from the National Research Foundation
 471 (NRF2015NRF-POC001-019) to N-J.C, and Swedish Research Council (2014-5557) and Swedish
 472 Foundation for Strategic Research (RMA11-0104) 533 to F.H.

473 **References**

- 474 1. Cornell, B.; Fletcher, G.; Middlehurst, J.; Separovic, F. The lower limit to the size of small
 475 sonicated phospholipid vesicles. *Biochim. Biophys. Acta, Biomembr.* 1982, 690, 15-19.
- 476 2. Walde, P.; Cosentino, K.; Engel, H.; Stano, P. Giant vesicles: preparations and applications.
 477 *ChemBioChem* 2010, 11, 848-865.
- 478 3. Rizo, J.; Rosenmund, C. Synaptic vesicle fusion. *Nat. Struct. Mol. Biol.* 2008, 15, 665-674.
- 479 4. Rizzoli, S. O.; Betz, W. J. Synaptic vesicle pools. *Nat. Rev. Neurosci.* 2005, 6, 57-69.
- 480 5. Fuhrmann, G.; Herrmann, I. K.; Stevens, M. M. Cell-derived vesicles for drug therapy and
 481 diagnostics: Opportunities and challenges. *Nano Today* 2015, 10, 397-409.
- 482 6. Ostro, M. J. *Liposomes: from biophysics to therapeutics*. Courier Corporation: 1987.
- 483 7. Torchilin, V. P. Recent advances with liposomes as pharmaceutical carriers. *Nat. Rev. Drug*
 484 *Discov.* 2005, 4, 145-160.
- 485 8. Barenholz, Y. Liposome application: problems and prospects. *Curr. Opin. Colloid Interface*
 486 *Sci.* 2001, 6, 66-77.
- 487 9. Chatin, B.; Mevel, M.; Devalliere, J.; Dallet, L.; Haudebourg, T.; Peuziat, P.; Colombani, T.;
 488 Berchel, M.; Lambert, O.; Edelman, A.; Pitard, B. Liposome-based Formulation for Intracellular
 489 Delivery of Functional Proteins. *Mol Ther Nucleic Acids* 2015, 4, e244.
- 490 10. Tabaei, S. R.; Rabe, M.; Zetterberg, H.; Zhdanov, V. P.; Höök, F. Single lipid vesicle assay
 491 for characterizing single-enzyme kinetics of phospholipid hydrolysis in a complex biological fluid.
 492 *J. Am. Chem. Soc.* 2013, 135, 14151-14158.
- 493 11. Rabe, M.; Tabaei, S. R.; Zetterberg, H.; Zhdanov, V. P.; Höök, F. Hydrolysis of a lipid
 494 membrane by single enzyme molecules: accurate determination of kinetic parameters. *Angew.*
 495 *Chem. Int. Ed. Engl.* 2015, 54, 1022-1026.
- 496 12. Hatzakis, N. S.; Bhatia, V. K.; Larsen, J.; Madsen, K. L.; Bolinger, P.-Y.; Kunding, A. H.;
 497 Castillo, J.; Gether, U.; Hedegård, P.; Stamou, D. How curved membranes recruit amphipathic
 498 helices and protein anchoring motifs. *Nat. Chem. Biol.* 2009, 5, 835-841.
- 499 13. Tabaei, S. R.; Rabe, M.; Zhdanov, V. P.; Cho, N.-J.; Höök, F. Single vesicle analysis reveals
 500 nanoscale membrane curvature selective pore formation in lipid membranes by an antiviral α -
 501 helical peptide. *Nano Lett.* 2012, 12, 5719-5725.
- 502 14. Jackman, J. A.; Saravanan, R.; Zhang, Y.; Tabaei, S. R.; Cho, N. J. Correlation between
 503 Membrane Partitioning and Functional Activity in a Single Lipid Vesicle Assay Establishes Design
 504 Guidelines for Antiviral Peptides. *Small* 2015, 11, 2372-2379.
- 505 15. Leitenberger, S. M.; Reister-Gottfried, E.; Seifert, U. Curvature coupling dependence of
 506 membrane protein diffusion coefficients. *Langmuir* 2008, 24, 1254-1261.
- 507 16. Helfrich, W. Elastic properties of lipid bilayers: theory and possible experiments. *Zeitschrift*
 508 *für Naturforschung C* 1973, 28, 693-703.
- 509 17. Gruner, S. M. Stability of lyotropic phases with curved interfaces. *J Phys Chem* 1989, 93,
 510 7562-7570.
- 511 18. Tian, A.; Capraro, B. R.; Esposito, C.; Baumgart, T. Bending stiffness depends on curvature
 512 of ternary lipid mixture tubular membranes. *Biophys. J.* 2009, 97, 1636-1646.

- 513 19. Seifert, U. Curvature-induced lateral phase segregation in two-component vesicles. *Phys.*
514 *Rev. Lett.* 1993, 70, 1335.
- 515 20. Oussoren, C.; Zuidema, J.; Crommelin, D.; Storm, G. Lymphatic uptake and biodistribution
516 of liposomes after subcutaneous injection.: II. Influence of liposomal size, lipid composition and
517 lipid dose. *Biochim. Biophys. Acta, Biomembr.* 1997, 1328, 261-272.
- 518 21. Lohse, B.; Bolinger, P.-Y.; Stamou, D. Encapsulation efficiency measured on single small
519 unilamellar vesicles. *J. Am. Chem. Soc.* 2008, 130, 14372-14373.
- 520 22. Huang, W.-C.; Burnouf, P.-A.; Su, Y.-C.; Chen, B.-M.; Chuang, K.-H.; Lee, C.-W.; Wei, P.-
521 K.; Cheng, T.-L.; Roffler, S. R. Engineering Chimeric Receptors to Investigate the Size and
522 Rigidity-Dependent Interaction of PEGylated Nanoparticles with Cells. *ACS nano* 2016.
- 523 23. Rahman, Y.; Cerny, E.; Patel, K.; Lau, E.; Wright, B. Differential uptake of liposomes
524 varying in size and lipid composition by parenchymal and Kupffer cells of mouse liver. *Life Sci.*
525 1982, 31, 2061-2071.
- 526 24. Allen, T.; Austin, G.; Chonn, A.; Lin, L.; Lee, K. Uptake of liposomes by cultured mouse
527 bone marrow macrophages: influence of liposome composition and size. *Biochim. Biophys. Acta,*
528 *Biomembr.* 1991, 1061, 56-64.
- 529 25. Zhang, S.; Gao, H.; Bao, G. Physical principles of nanoparticle cellular endocytosis. *ACS*
530 *nano* 2015, 9, 8655-8671.
- 531 26. Yan, Y.; Such, G. K.; Johnston, A. P.; Best, J. P.; Caruso, F. Engineering particles for
532 therapeutic delivery: prospects and challenges. *ACS nano* 2012, 6, 3663-3669.
- 533 27. Wang, B.; Anthony, S. M.; Bae, S. C.; Granick, S. Anomalous yet brownian. *Proc. Natl.*
534 *Acad. Sci. USA* 2009, 106, 15160-15164.
- 535 28. Wong, I.; Gardel, M.; Reichman, D.; Weeks, E. R.; Valentine, M.; Bausch, A.; Weitz, D.
536 Anomalous diffusion probes microstructure dynamics of entangled F-actin networks. *Phys. Rev.*
537 *Lett.* 2004, 92, 178101.
- 538 29. Mason, T. G.; Weitz, D. Optical measurements of frequency-dependent linear viscoelastic
539 moduli of complex fluids. *Phys. Rev. Lett.* 1995, 74, 1250.
- 540 30. Cheung, C.; Hwang, Y.; Wu, X.; Choi, H. Diffusion of particles in free-standing liquid
541 films. *Phys. Rev. Lett.* 1996, 76, 2531.
- 542 31. Ewers, H.; Smith, A. E.; Sbalzarini, I. F.; Lilie, H.; Koumoutsakos, P.; Helenius, A. Single-
543 particle tracking of murine polyoma virus-like particles on live cells and artificial membranes. *Proc.*
544 *Natl. Acad. Sci. USA* 2005, 102, 15110-15115.
- 545 32. Hormel, T. T.; Kurihara, S. Q.; Brennan, M. K.; Wozniak, M. C.; Parthasarathy, R.
546 Measuring lipid membrane viscosity using rotational and translational probe diffusion. *Phys. Rev.*
547 *Lett.* 2014, 112, 188101.
- 548 33. Lee, G. M.; Ishihara, A.; Jacobson, K. A. Direct observation of Brownian motion of lipids in
549 a membrane. *Proc. Natl. Acad. Sci. USA* 1991, 88, 6274-6278.
- 550 34. Nguyen, Z. H.; Atkinson, M.; Park, C. S.; Maclennan, J.; Glaser, M.; Clark, N. Crossover
551 between 2D and 3D fluid dynamics in the diffusion of islands in ultrathin freely suspended smectic
552 films. *Phys. Rev. Lett.* 2010, 105, 268304.
- 553 35. Lohr, C.; Kunding, A. H.; Bhatia, V. K.; Stamou, D. Constructing size distributions of
554 liposomes from single-object fluorescence measurements. *Methods Enzymol.* 2009, 465, 143-160.
- 555 36. Yoshina-Ishii, C.; Boxer, S. G. Controlling two-dimensional tethered vesicle motion using
556 an electric field: interplay of electrophoresis and electro-osmosis. *Langmuir* 2006, 22, 2384-2391.
- 557 37. Jönsson, P.; Jönsson, B. Hydrodynamic forces on macromolecules protruding from lipid
558 bilayers due to external liquid flows. *Langmuir* 2015, 31, 12708-12718.
- 559 38. Block, S.; Fast, B. J.; Lundgren, A.; Zhdanov, V. P.; Höök, F. Two-Dimensional Flow
560 Nanometry of Biological Nanoparticles for Accurate Determination of Their Size and Emission
561 Intensity. *arXiv preprint arXiv:1604.06077* 2016.
- 562 39. Block, S.; Zhdanov, V. P.; Höök, F. Quantification of Multivalent Interactions by Tracking

563 Single Biological Nanoparticle Mobility on a Lipid Membrane. *Nano Lett.* 2016.
564 40. Joseph M. Johnson; Taekjip Ha; Steve Chu; Boxer, S. G. Early Steps of Supported Bilayer
565 Formation Probed by Single Vesicle Fluorescence Assays. *Biophys. J.* 2002, 83, 3371–3379.
566 41. Jackman, J. A.; Špačková, B.; Linardy, E.; Kim, M. C.; Yoon, B. K.; Homola, J.; Cho, N.-J.
567 Nanoplasmonic ruler to measure lipid vesicle deformation. *Chem. Commun.* 2016, 52, 76-79.
568 42. Schönherr, H.; Johnson, J. M.; Lenz, P.; Frank, C. W.; Boxer, S. G. Vesicle Adsorption and
569 Lipid Bilayer Formation on Glass Studied by Atomic Force Microscopy. *Langmuir* 2004, 20,
570 11600-11606.
571 43. Hain, N.; Gallego, M.; Reviakine, I. Unraveling supported lipid bilayer formation kinetics:
572 osmotic effects. *Langmuir* 2013, 29, 2282-2288.
573 44. Jackman, J. A.; Zan, G. H.; Zhao, Z.; Cho, N.-J. Contribution of the hydration force to
574 vesicle adhesion on titanium oxide. *Langmuir* 2014, 30, 5368-5372.
575 45. Oh, E.; Jackman, J. A.; Yorulmaz, S.; Zhdanov, V. P.; Lee, H.; Cho, N.-J. Contribution of
576 Temperature to Deformation of Adsorbed Vesicles Studied by Nanoplasmonic Biosensing.
577 *Langmuir* 2015, 31, 771-781.
578 46. Jackman, J. A.; Tabaei, S. R.; Zhao, Z.; Yorulmaz, S.; Cho, N.-J. Self-assembly formation of
579 lipid bilayer coatings on bare aluminum oxide: overcoming the force of interfacial water. *ACS Appl.*
580 *Mater. Interfaces* 2014, 7, 959-968.
581 47. Solon, J.; Pécréaux, J.; Girard, P.; Fauré, M.-C.; Prost, J.; Bassereau, P. Negative tension
582 induced by lipid uptake. *Phys. Rev. Lett.* 2006, 97, 098103.
583 48. Kunze, A.; Svedhem, S.; Kasemo, B. Lipid transfer between charged supported lipid
584 bilayers and oppositely charged vesicles. *Langmuir* 2009, 25, 5146-5158.
585 49. O'Neill, M. A sphere in contact with a plane wall in a slow linear shear flow. *Chem. Eng.*
586 *Sci.* 1968, 23, 1293-1298.
587 50. Filipe, V.; Hawe, A.; Jiskoot, W. Critical evaluation of Nanoparticle Tracking Analysis
588 (NTA) by NanoSight for the measurement of nanoparticles and protein aggregates. *Pharm. Res.*
589 2010, 27, 796-810.
590 51. Lipowsky, R.; Seifert, U. Adhesion of vesicles and membranes. *Mol. Cryst. Liq. Cryst.*
591 1991, 202, 17-25.
592 52. Reviakine, I.; Gallego, M.; Johannsmann, D.; Tellechea, E. Adsorbed liposome deformation
593 studied with quartz crystal microbalance. *J. Chem. Phys.* 2012, 136, 084702.
594 53. Seifert, U. Configurations of fluid membranes and vesicles. *Adv. Phys.* 1997, 46, 13-137.
595 54. Dimitrievski, K. Deformation of adsorbed lipid vesicles as a function of vesicle size.
596 *Langmuir* 2010, 26, 3008-3011.
597 55. Jackman, J. A.; Zhdanov, V. P.; Cho, N.-J. Nanoplasmonic Biosensing for Soft Matter
598 Adsorption: Kinetics of Lipid Vesicle Attachment and Shape Deformation. *Langmuir* 2014, 30,
599 9494-9503.
600 56. Olsson, T.; Zhdanov, V. P.; Höök, F. Total internal reflection fluorescence microscopy for
601 determination of size of individual immobilized vesicles: Theory and experiment. *J. Appl. Phys*
602 2015, 118, 064702.
603 57. Biltonen, R. L.; Lichtenberg, D. The use of differential scanning calorimetry as a tool to
604 characterize liposome preparations. *Chem Phys Lipids* 1993, 64, 129-142.
605 58. Lee, C.-H.; Lin, W.-C.; Wang, J. All-optical measurements of the bending rigidity of lipid-
606 vesicle membranes across structural phase transitions. *Phys. Rev. E* 2001, 64, 020901.
607 59. Pan, J.; Mills, T. T.; Tristram-Nagle, S.; Nagle, J. F. Cholesterol perturbs lipid bilayers
608 nonuniversally. *Phys. Rev. Lett.* 2008, 100, 198103.
609 60. Seifert, U. Hydrodynamic lift on bound vesicles. *Phys. Rev. Lett.* 1999, 83, 876.
610 61. Saffman, P. The lift on a small sphere in a slow shear flow. *J. Fluid Mech.* 1965, 22, 385-
611 400.
612 62. Asakura, S.; Oosawa, F. On interaction between two bodies immersed in a solution of

613 macromolecules. *J. Chem. Phys* 1954, 22, 1255-1256.
614 63. Yoshina-Ishii, C.; Chan, Y.-H. M.; Johnson, J. M.; Kung, L. A.; Lenz, P.; Boxer, S. G.
615 Diffusive dynamics of vesicles tethered to a fluid supported bilayer by single-particle tracking.
616 *Langmuir* 2006, 22, 5682-5689.
617 64. De Gier, J. Osmotic behaviour and permeability properties of liposomes. *Chem Phys Lipids*
618 1993, 64, 187-196.
619 65. Ohlsson, G.; Tabaei, S. R.; Beech, J.; Kvassman, J.; Johanson, U.; Kjellbom, P.; Tegenfeldt,
620 J. O.; Höök, F. Solute transport on the sub 100 ms scale across the lipid bilayer membrane of
621 individual proteoliposomes. *Lab Chip* 2012, 12, 4635-4643.
622 66. Brändén, M.; Tabaei, S. R.; Fischer, G.; Neutze, R.; Höök, F. Refractive-index-based
623 screening of membrane-protein-mediated transfer across biological membranes. *Biophys. J.* 2010,
624 99, 124-133.
625 67. Yang, K.; Ma, Y.-Q. Computer simulation of the translocation of nanoparticles with
626 different shapes across a lipid bilayer. *Nat. Nanotechnol.* 2010, 5, 579-583.
627 68. Tree-Udom, T.; Seemork, J.; Shigyou, K.; Hamada, T.; Sangphech, N.; Palaga, T.; Insin, N.;
628 Pan-In, P.; Wanichwecharungruang, S. Shape Effect on Particle-Lipid Bilayer Membrane
629 Association, Cellular Uptake, and Cytotoxicity. *ACS Appl. Mater. Interfaces* 2015, 7, 23993-24000.
630 69. Gratton, S. E.; Ropp, P. A.; Pohlhaus, P. D.; Luft, J. C.; Madden, V. J.; Napier, M. E.;
631 DeSimone, J. M. The effect of particle design on cellular internalization pathways. *Proc. Natl.*
632 *Acad. Sci. USA* 2008, 105, 11613-11618.
633 70. Wrobel, I.; Collins, D. Fusion of cationic liposomes with mammalian cells occurs after
634 endocytosis. *Biochim. Biophys. Acta, Biomembr.* 1995, 1235, 296-304.
635 71. Ewert, K.; Slack, N. L.; Ahmad, A.; Evans, H. M.; Lin, A. J.; Samuel, C. E.; Safinya, C. R.
636 Cationic lipid-DNA complexes for gene therapy: understanding the relationship between complex
637 structure and gene delivery pathways at the molecular level. *Curr. Med. Chem.* 2004, 11, 133-149.
638 72. McMahon, H. T.; Kozlov, M. M.; Martens, S. Membrane curvature in synaptic vesicle
639 fusion and beyond. *Cell* 2010, 140, 601-605.
640 73. Kawamoto, S.; Klein, M. L.; Shinoda, W. Coarse-grained molecular dynamics study of
641 membrane fusion: Curvature effects on free energy barriers along the stalk mechanism. *J. Chem.*
642 *Phys* 2015, 143, 243112.
643 74. Tabaei, S. R.; Gillissen, J.; Vafaei, S.; Groves, J. T.; Cho, N.-J. Size-Dependent, Stochastic
644 Nature of Lipid Exchange Between Nano-Vesicles and Model Membranes. *Nanoscale* 2016.
645
646